

## A high-performance carbon-carbon(C/C) Quasi-Solid-State Supercapacitor with Conducting Gel Electrolyte

Dexuan Wang<sup>1,\*</sup>, Liangmin Yu<sup>1,\*</sup>, Benlin He<sup>2</sup>, Lei Wang<sup>2</sup>

<sup>1</sup> Key Laboratory of Marine Chemistry Theory and Technology, Ministry of Education, Ocean University of China, Qingdao 266100, PR China;

<sup>2</sup> Institute of Materials Science and Engineering, Ocean University of China, Qingdao 266100, PR China;

\*E-mail: [wangdexuan@stu.ouc.edu.cn](mailto:wangdexuan@stu.ouc.edu.cn), [yuyan@ouc.edu.cn](mailto:yuyan@ouc.edu.cn)

Received: 13 December 2017 / Accepted: 17 January 2018 / Published: 5 February 2018

---

The development of the electric double-layer capacitors (EDLCs) that pursue for the advantages of easily carrying, no leaking and high capacitance has been a strong objective at the moment. Here a new type gel electrolyte with a high special conductivity of  $15.06 \text{ mS}\cdot\text{cm}^{-2}$  was fabricate by immersing polyacrylamide gel (PAM-G) matrix in 6 M KOH aqueous solution for 60 hours. As expected, the assembled quasi-solid-state supercapacitor based PAM-G electrolyte exhibits a specific capacitance (of  $196 \text{ F}\cdot\text{g}^{-1}$  and  $156 \text{ F}\cdot\text{g}^{-1}$  at the charge-discharge current density of  $1 \text{ A}\cdot\text{g}^{-1}$  and  $10 \text{ A}\cdot\text{g}^{-1}$ , respectively), maximum power of  $10 \text{ kW}\cdot\text{kg}^{-1}$  along with energy density of  $28.6 \text{ Wh}\cdot\text{kg}^{-1}$  (under the current density of  $10 \text{ A}\cdot\text{g}^{-1}$ ), and the capacitance retention rate keeps 98% after 5000 cycles at  $1 \text{ A}\cdot\text{g}^{-1}$ , demonstrating a high cycling stability, an excellent rate capability as well as a high specific capacitance of the device. The promising electrochemical performance could be attributed to the unique homogeneous and microporous three-dimensional structure of the PAM-G which can greatly enhance the permeability and transportation of different ions.

---

**Keywords:** Quasi-solid-state supercapacitors; PAM-G matrix; Three-dimensional structure; Energy storage

### 1. INTRODUCTION

Nowadays, the energy crisis and environmental pollution are becoming increasingly prominent issues not only because the major source of fossil fuels will be soon exhausted in the near future, but also the applications of the fossil fuels could seriously pollute the environment by discharging various compounds containing carbon, sulfur and dust [1-2]. In view of the above problems, there is high expectation for using new green energy to replace traditional fossil fuels as the main source of energy

in our daily life and industrial production [3-5]. Electric double-layer capacitors (EDLCs) which are also known as a unique class of electrical energy storage devices have attracted considerable attention in the fields of portable electronics [10], hybrid electric vehicles [11-12], and stand-by power systems [13] owing to their superior advantages such as high power density, rapid charging/discharging ability, and long cycle life [6-9]. The liquid electrolytes which are commonly used in the traditional EDLCs have several problems such as easily leaking, carrying difficulty and adapting to a narrow temperature range [14-19]. Polymer gel electrolyte integrated the advantages of rapid ions transmission of the liquid electrolyte and high stability of the full-solid-state electrolytes [20-22] has been extensively reviewed to solve these problems [23-26]. For example, a new EMIMCl/water gel was obtained by self-triggered UV polymerization and applied to the supercapacitor as the electrolyte accompanying specific capacitance of  $136 \text{ F}\cdot\text{g}^{-1}$  at the electric current density of  $0.5 \text{ A}\cdot\text{g}^{-1}$  [27]. A different kind of proton source and diphenyl phosphate has been used to fabricate proton-conducting gel polymer electrolyte which used in the supercapacitors showing high stability and an extreme temperature range between  $-40 \text{ }^\circ\text{C}$  and  $80 \text{ }^\circ\text{C}$  (the capacitance reached  $80 \text{ F}\cdot\text{g}^{-1}$  at  $-40 \text{ }^\circ\text{C}$  and the obtained capacitance about  $133 \text{ F}\cdot\text{g}^{-1}$  at  $80 \text{ }^\circ\text{C}$ ) [28]. More recently, intensive efforts have been devoted to various gel polymer electrolyte systems for flexible SCs, such as PVA-acid or alkali [29-32], polyethylene oxide (PEO)-alkali [33], potassium polyacrylate (PAAK)-salt or alkali [34-35].

In this work, the PAM-G matrix has been synthesized by aqueous solution polymerization, and then immersed into 6 M KOH aqueous solution soaking for different time to fabricate gel electrolyte with the advantages of high conductivity and considerable mechanical properties. The PAM-G has a typical three-dimensional (3D) network structure with a suitable degree of crosslinking accompanying with simple and low cost of synthesis process. Not only it is able to absorb a large amount of KOH solution governed by osmotic pressure and capillary force across the membrane and micropores to form a stable structure, but also the absorbed ions are hardly removed under some pressure [36]. The N-H of  $-\text{CONH}_2$  is substituted by  $-\text{OH}$  under the condition of alkaline solutions, the new formed  $-\text{COOH}$  can react with KOH, and then  $\text{K}^+$  can be wrapped in the three-dimensional structure of the PAM-G [37]. The prepared PAM-G electrolyte has been then coupled with activated carbon electrodes to assemble a simple quasi-solid-state supercapacitor device. The quasi-solid-state electrolytes have good application prospects because of better capacity and stability by analyzing the electrochemical performances of the composed supercapacitor.

## 2. EXPERIMENTAL PROCEDURE

### 2.1. Synthesis of PAM-G composites

The PAM-G matrices were synthesized in a method of aqueous polymerization route. In a typical synthesis, 10 g of acrylamide monomer were dissolved into 15 mL of deionized water under magnetic stirring for 15 minutes. After fully dissolved, 0.0015 g of N,N'-(methylene) bisacrylamide and 0.06 g of ammonium persulfate were successively added into the above solution. When the above preparatory work was completed, the reactant was slowly heated in a water bath of  $80 \text{ }^\circ\text{C}$  accompanied

by stirring. As the polymerization reaction was carried out slowly, the viscosity of the reactant increased gradually. When the viscosity of the PAM polymers achieved around  $185 \text{ mPa}\cdot\text{s}^{-1}$ , the product was quickly transferred to a petri dish and cooled to  $25 \text{ }^\circ\text{C}$  under the condition of ice water with the formation of an elastic white gel. After being rinsed with ultra-pure water, the products were cut into small squares of  $1 \times 1 \text{ cm}^2$  and dried at  $80 \text{ }^\circ\text{C}$  for more than 12 h.

## 2.2. Preparation of conducting PAM-G electrolytes

The microporous PAM-G matrices were prepared by immersing dried PAM-G matrices in deionized water for 72 h to reach their swelling equilibrium, and subsequently freeze-dried under vacuum at  $-60 \text{ }^\circ\text{C}$  for 72 h. In order to obtain the gel electrolytes, the dried microporous PAM-G were immersed in 6 M KOH aqueous solution for 60 hours to reach their swelling equilibriums. Under the condition of absorption balance, the  $\text{K}^+$  and  $\text{OH}^-$  of the solution will be reserved in the 3D frameworks of gels to form the PAM-G electrolytes.

## 2.3. Synthesis of the activated carbon electrode

To get the working electrode, the carbon material powders were mixed with black lead and polytetrafluoroethylene at a mass ratio of 8:1:1. A small amount of ethanol was added into the obtained powder to form homogenous solution by stirring. The mixture was pressed on nickel foam ( $1 \times 1 \text{ cm}^2$ ) and kept for 40 s, and then the obtained working electrodes were dried at  $80 \text{ }^\circ\text{C}$  in an oven for 12 h.

## 2.4. The assembly of PAM-G supercapacitor

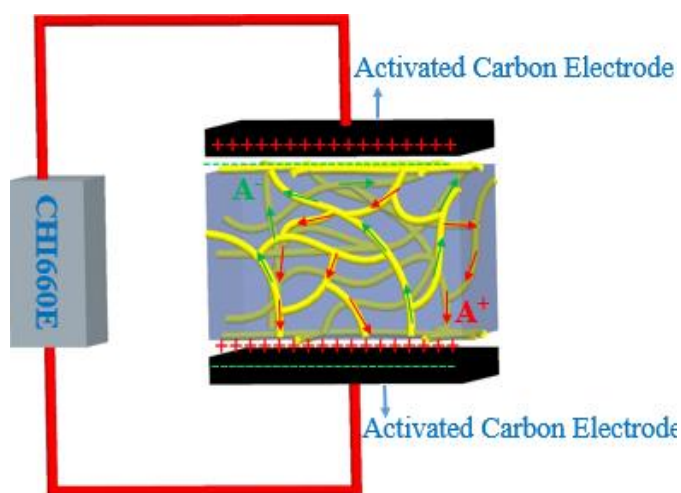


**Figure 1.** Schematic representation of the quasi-solid-state supercapacitor.

The activated carbon electrode about  $1 \pm 0.2 \text{ mg}$  and PAM-G/graphite electrolyte with the thickness of  $0.5 \text{ cm}$  and geometrical area of  $2 \times 2 \text{ cm}^2$  were prepared in the preliminary stage. As shown in Fig. 1, the quasi-solid-state supercapacitor consists of two equal quantity activated carbon electrodes

and the PAM-G electrolyte which acts as separator and electrolyte. We call this combination of the supercapacitor dubbed the sandwich combinations.

### 2.5. Characterization

The morphologies and sizes of the PAM-G matrices were determined by field-emission scanning electron microscope (FE-SEM JSM 6700F). To observe the internal 3D microstructure, swollen gel electrolytes were first cut into ultrathin film, followed by the loading into a chamber under freezing temperature and high vacuum to remove solvent. The ionic conductivities of the PAM-G electrolytes were recorded using a pocket conductivity meter (DSSJ-308A, Leici Instrument) by filling the gel electrolytes into the interspace between two electrodes. Before the experiments, the instrument was calibrated with 0.01 M KCl aqueous solution. Fourier transform infrared spectrometry (FTIR) spectra were recorded on a Vertex 70 FTIR spectrometer (Bruker). The performance test of the supercapacitor such as cyclic voltammetry (CV), galvanostatic charge/discharge measurement and electrochemical impedance measurement (frequency range from 0.01 Hz to  $10^6$  Hz), was conducted with an electrochemical work station (CHI660E) under the potential window from 0 to 1 V. The long-term cycling stability of the supercapacitor was studied by electrochemical work station (CT2001A) at a current density of  $1 \text{ A}\cdot\text{g}^{-1}$ .

## 3. RESULTS AND DISCUSSION

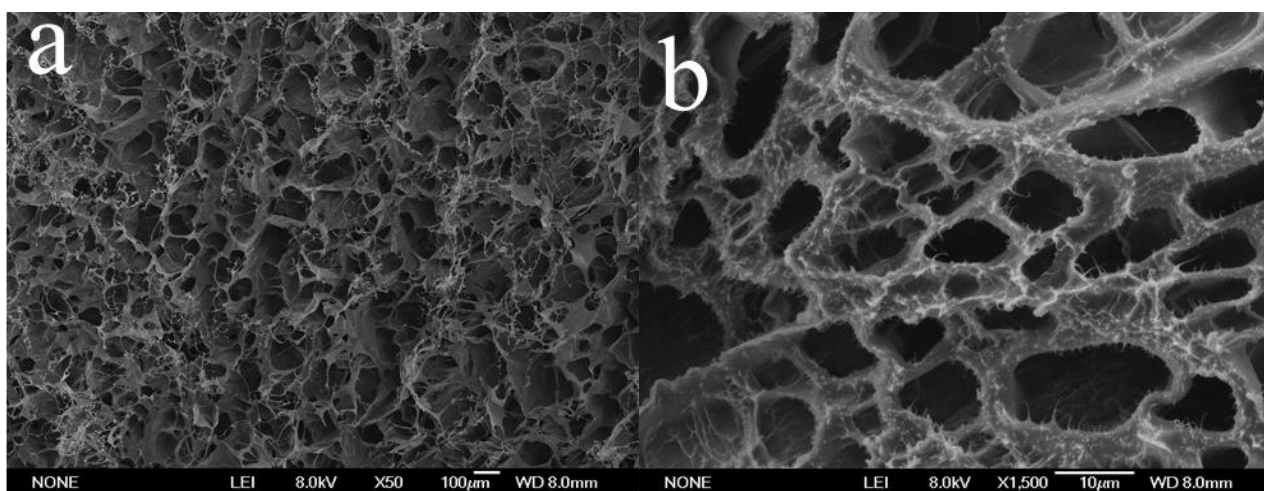


**Figure 2.** SEM images of microporous PAM-G matrix.

In order to study the internal structure of the PAM-G matrices, the SEM scanning was performed after the dense matrices were swollen in deionized water and subsequently freeze-dried at  $-60^\circ\text{C}$ . A distinctive structure with homogeneous and microporous three-dimensional framework can be found as shown in Fig. 2. Under the action of osmotic pressure and capillary diffusion from micropores, the porous three-dimensional structure can quickly cage more electrolyte than other

structure and facilitate the movement of different ions. At the same time, the photos of the prepared, dried and soaked in 6 M KOH aqueous solution for different time of PAM-G were illustrated in Fig. 3, the volume of the dried PAM-G gradually becomes larger with the increase of the absorption time, indicating that the quantity of incorporated  $K^+$  and  $OH^-$  is improved. When the soaked time is 66 h, the surface of the PAM-G matrix will become sticky indicated that the interior 3D structure of the newly formed gel electrolyte may have been collapsed under the condition of alkali solution.

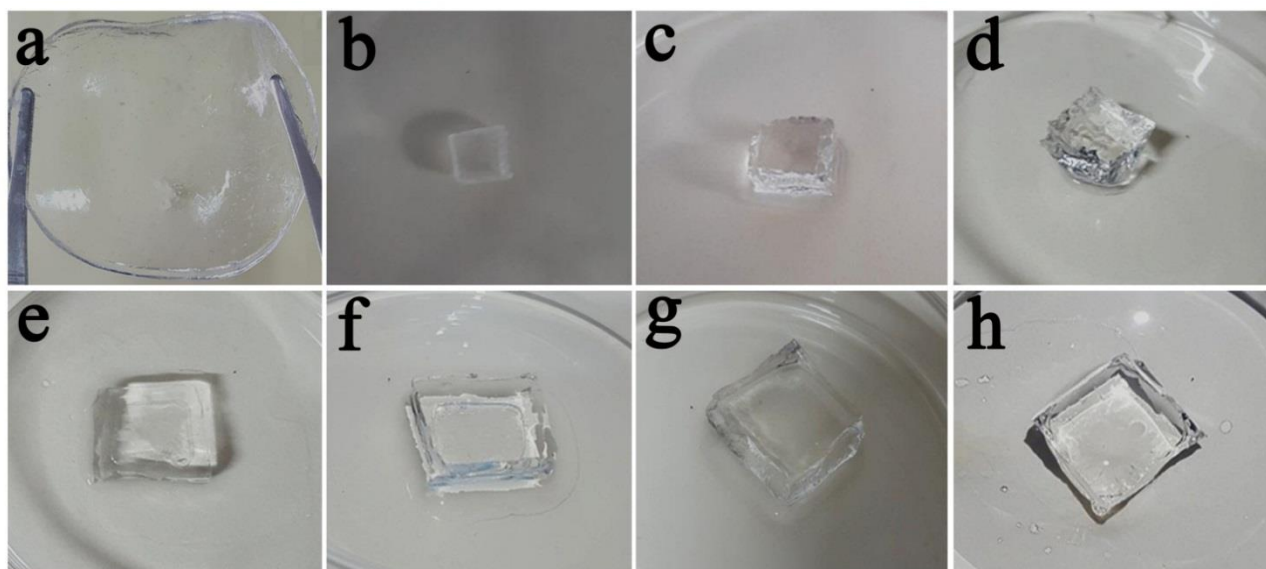


**Figure 3.** Photo images of the PAM-G matrix under different condition (a) just synthesized, (b) after dried, (c)-(h) soaked in 6 M KOH aqueous solution for 12, 24, 36, 48, 60, 66 h, respectively.

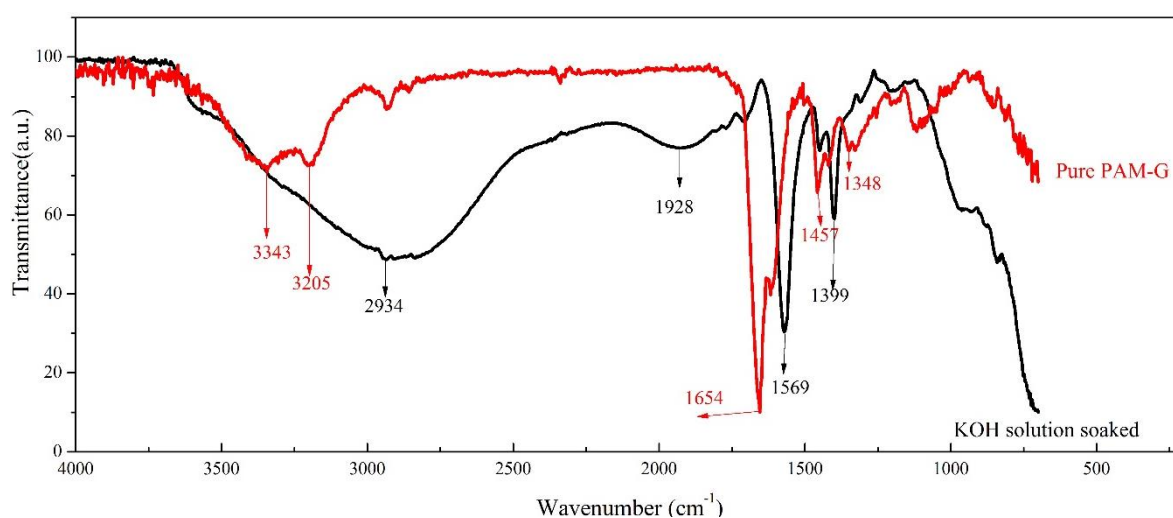


**Figure 4.** FTIR spectra of PAM-G and PAM-G electrolyte.

Infrared spectrography is a useful technique in characterizing structures of materials. It can be seen from Fig. 4, the peaks at  $\sim 3343$  and  $3205\text{ cm}^{-1}$  are attributed to N-H stretching mode for the

PAM-G and the peak at  $\sim 2934\text{ cm}^{-1}$  is corresponding to  $-\text{OH}$  stretching mode of the PAM-G after absorbed in the 6 M KOH aqueous solution. This phenomenon can be interpreted as that the  $\text{N-H}$  of  $-\text{CONH}_2$  is substituted by  $-\text{OH}$  under the condition of strong alkaline solutions. The new formed  $-\text{COOH}$  can react with the KOH solution, and then  $\text{K}^+$  and  $\text{OH}^-$  can be successfully incorporated into the PAM-G with three-dimensional ordered gel structure. The PAM-G can store enough  $\text{K}^+$  and  $\text{OH}^-$  to improve the charge and discharge capacity of the quasi-solid-state supercapacitor when it reaches equilibrium state in the solution for the reason. The peaks at  $1654, 1457\text{ cm}^{-1}$  and  $1568, 1399\text{ cm}^{-1}$  are precise assigned to the  $-\text{CONH}_2$  for the two different states of PAM-G, respectively. By comparison of two cases of PAM-G, it can be clearly seen that the  $-\text{NH}_2$  is not completely replaced by  $-\text{OH}$ . During the long time substituted all  $\text{N-H}$  by  $-\text{OH}$ , the three-dimensional structure of PAM-G will be damaged by the corrosion effect of strong alkaline solution, resulting in a reduction in the capacitance of the quasi-solid-state supercapacitor because of impeding the effective transportation of ions by the collapse structure. According to the FTIR analysis, a suitable absorption time of the PAM-G soak in the 6 M KOH aqueous solution is important for assembling the quasi-solid-state supercapacitor with perfect performance.

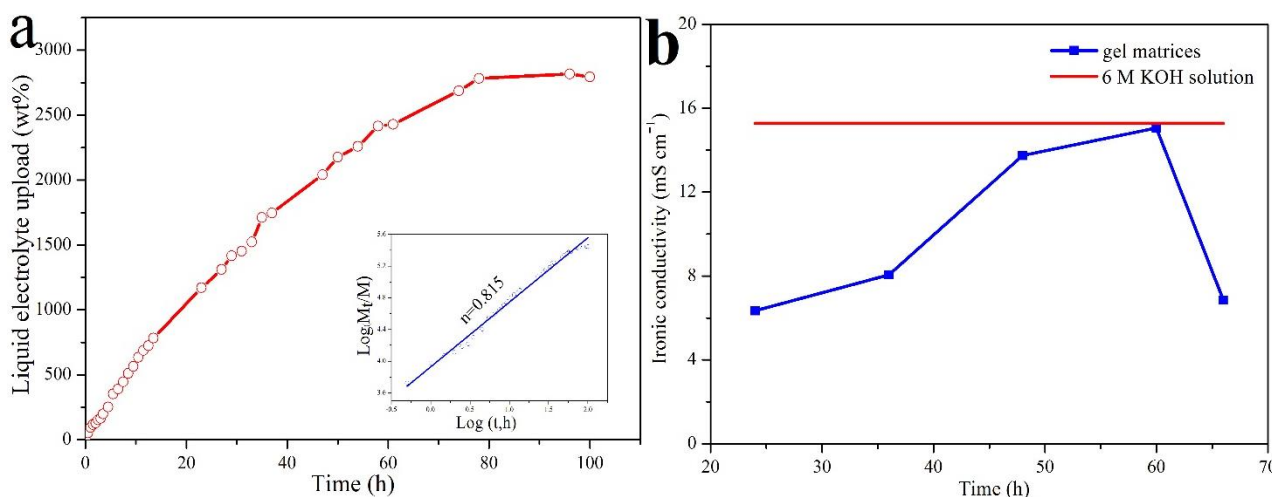


**Figure 5.** (a) The time dependences of 6 M KOH aqueous solution loading for pure PAM-G matrix, (b) Ionic conductivity for different states of PAM-G electrolyte.

Fig. 5a shows the imbibition kinetics of PAM-G matrix in the 6 M KOH aqueous solution which provides ions migration in the gel electrolyte. Under normal conditions, the swelling of PAM-G in liquid electrolyte obeys Flory theory. The relationship between the accumulative amount of liquid electrolyte loading and the imbibition time has been matched to investigate the imbibition mechanism by the Fickian theory [38]:

$$\frac{M_t}{M_\infty} = kt^n \tag{1}$$

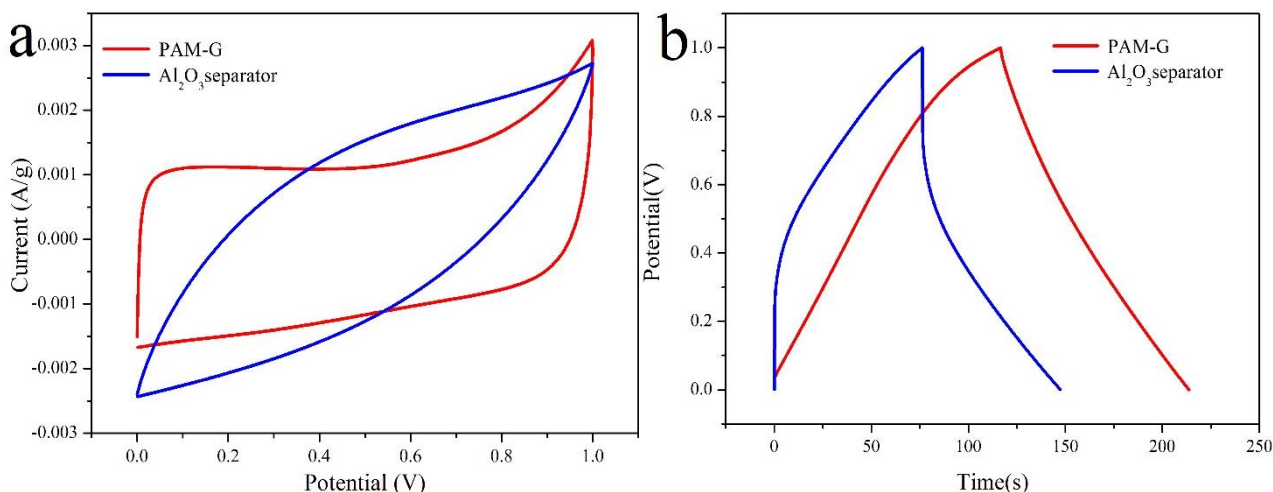
where  $M_t$  and  $M_\infty$  are the different masses of gel which imbibed KOH aqueous solution at time  $t$  and at equilibrium, respectively,  $k$  is a characteristic rate constant relating to the properties of gel

matrix, and  $n$  is a transport number characterizing the transport mechanism. According to the plots of  $\log(M_t/M_\infty) - \log(t)$  and extracted  $n$  values in Fig. 5a, the  $n$  value from the PAM-G matrix by swelling in 6 M KOH aqueous solution is 0.815 more higher than 0.5, indicating an anomalous mechanism mode in which structural relaxation is comparable to diffusion [39]. The result indicates that the loading of liquid electrolyte is controlled by osmotic pressure and capillary diffusion. The swelling of a gel matrix in the KOH aqueous solution can be divided into three steps: (i)  $K^+$  and  $OH^-$  enter gel matrix, (ii) relaxation of the different ions, and (iii) the equilibrium of PAM-G. The liquid electrolyte loading can be obtained according to the equation:

$$\text{Liquid electrolyte loading} = \frac{M_{\text{gel}} - M_{\text{matrix}}}{M_{\text{matrix}}} \times 100\% \quad (2)$$

Where  $M_{\text{gel}}$  (g) and  $M_{\text{matrix}}$  (g) are masses of polymer gel electrolyte and anhydrous polymer matrix, respectively. A significant increase of liquid electrolyte loading within 60 hours shows a wonderful ability of PAM-G toward KOH solution, yielding a final liquid electrolyte loading of 2435wt%. The surface of the PAM-G becomes sticky accompanying the internal structure may have been destroyed due to the high concentration of KOH solution when the soaking time is more than 60 hours. The incorporation result shows that the 3D PAM-G provides a good framework for reserving and migrating liquid electrolyte.

The Ionic conductivity of the PAM-G caging 6 M KOH solution for different time was shown in Fig. 5b, suggesting that the conductivity of the PAM-G electrolyte increased or reduced when the soaking time is less or more than 60 h. In comparison with  $15.28 \text{ mS}\cdot\text{cm}^{-2}$  for 6 M KOH aqueous solution, the conductivity of the PAM-G matrices sucked with 6 M KOH aqueous solution for 60 h is almost reach  $15.06 \text{ mS}\cdot\text{cm}^{-2}$ . As can be seen from the above data, it is reasonable to select 60 h as the absorption time for the PAM-G matrix immersing into the 6 M KOH aqueous solution to obtain the quasi-solid electrolyte. In order to investigate the differences between the quasi-solid-state supercapacitor with PAM-G electrolyte and the supercapacitor with  $\text{Al}_2\text{O}_3$  diaphragm, CV, galvanostatic charge/discharge and EIS experiments were further performed at a voltage window of 0-1 V, as shown in Fig. 6. Fig. 6a shows the CV curves of two different electrolyte of the supercapacitor at a scan rate of  $10 \text{ mV}\cdot\text{s}^{-1}$ .



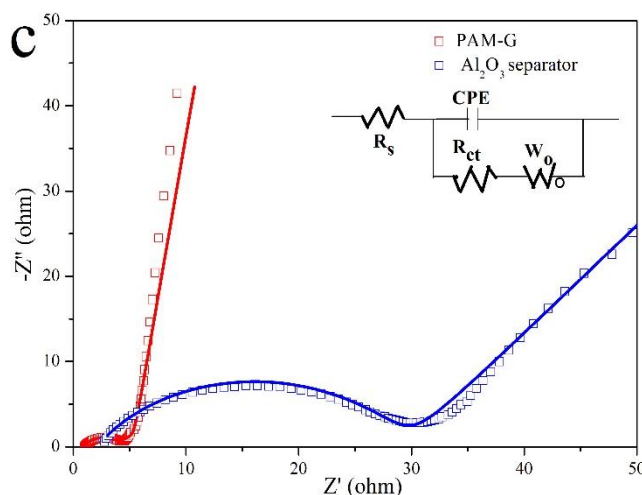
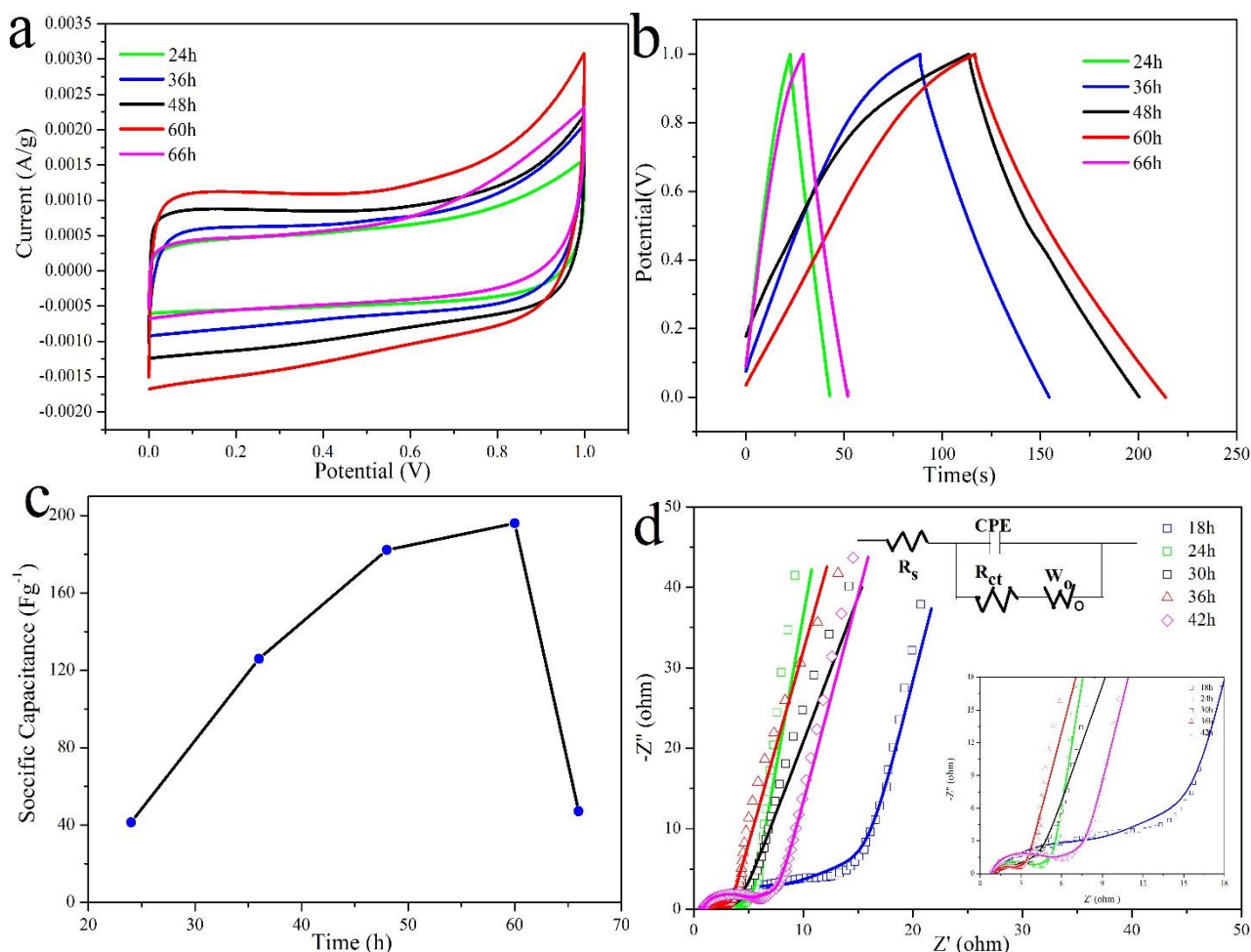


**Figure 6.** (a) CV curves at a scan rate of  $10 \text{ mV}\cdot\text{s}^{-1}$ , (b) Galvanostatic charge-discharge profile at current densities of  $1 \text{ A}\cdot\text{g}^{-1}$ , (c) Nyquist plots of the two types of supercapacitors.

The CV curve of the quasi-solid-state supercapacitor with PAM-G electrolyte shows more standard quasi-rectangular shape and large area than that of the supercapacitor with  $\text{Al}_2\text{O}_3$  separator indicating typical electrical double layer capacitive behavior and better performance of the quasi-solid-state supercapacitor. The capacitive performance was further evaluated using the following equation [40] in the two-electrode system:

$$C_s = \frac{2I}{(dV/dt)m} \quad (3)$$

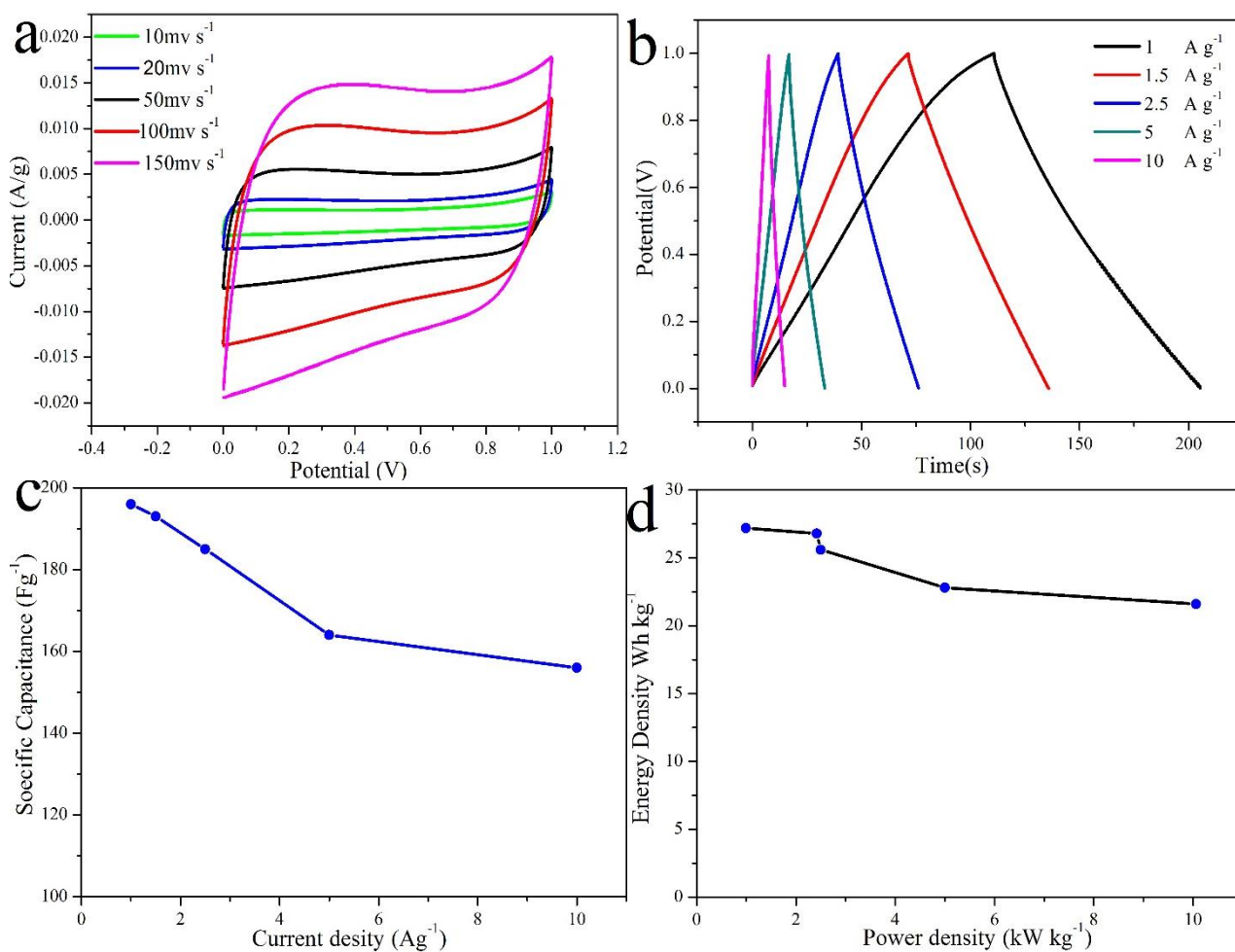
where  $I$  is the current (A),  $dV/dt$  is the slope of the discharge curve after the ohmic drop ( $\text{V}\cdot\text{s}^{-1}$ ), and  $m$  is the mass (g) of active material in each electrode. Fig. 6b shows the comparative charge-discharge curves for the two different kinds of supercapacitors at a current density of  $1 \text{ A}\cdot\text{g}^{-1}$ . As shown in the figure, the  $C_s$  of quasi-solid-state supercapacitor with PAM-G electrolyte is  $196 \text{ F}\cdot\text{g}^{-1}$  much higher than  $142 \text{ F}\cdot\text{g}^{-1}$  of the supercapacitor with  $\text{Al}_2\text{O}_3$  separator, suggesting that the quasi-solid-state supercapacitor with PAM-G electrolyte offers a much larger capacitance, which agrees well with the obtained results from CV tests. As shown in Fig. 6c, the Nyquist plots of the two different styles supercapacitor show a partial semicircle at high frequency and a straight line at low frequency, corresponding to the charge transfer resistance and capacitive behavior, respectively. The straight line of the quasi-solid-state supercapacitor with PAM-G electrolyte is almost vertical, indicating a better capacitive behavior. The charge transfer resistance ( $R_{ct}$ ) of the quasi-solid-state supercapacitor with PAM-G electrolyte is simulated to be  $1.153 \Omega$ , which is smaller than  $27.2 \Omega$  of the supercapacitor with  $\text{Al}_2\text{O}_3$  separator. From the above results, it can be convinced that the quasi-solid-state supercapacitor with PAM-G electrolyte has a much better electrochemical performance than the supercapacitor with  $\text{Al}_2\text{O}_3$  separator.



**Figure 7.** (a) CV curves at a scan rate of  $10 \text{ mV}\cdot\text{s}^{-1}$ , (b) Galvanostatic charge–discharge profile at current densities of  $1 \text{ A}\cdot\text{g}^{-1}$ , (c) Specific capacitance and (d) Nyquist plots of the quasi-solid-state supercapacitor with the PAM-G soaking for 24, 36, 48, 60 and 66 h, respectively.

The CV curves of the quasi-solid-state supercapacitor which using PAM-G soaking in 6 M KOH solution with different time as electrolyte at a scan rate of  $10 \text{ mV}\cdot\text{s}^{-1}$  was shown in Fig. 7a. The area of the unique quasi-rectangular shape gradually increases within the absorption time of 60 hours and reduces when the soaking time is longer than 60 h, which is perfect matching the triangles of the galvanostatic charge/discharge curves at a current density of  $1 \text{ A}\cdot\text{g}^{-1}$  shown in Fig. 7b. At the same time, the variation of capacitances with the PAM-G soaked in 6 M KOH aqueous solution for different time was shown in Fig. 7c. As can be seen from the figure, the capacitance of the quasi-solid-state supercapacitor gradually increases within the caging time of 60 h and rapidly decreased when the soaking time attains 66 h. Such capacitance change accompanying different soaking time matches the absorption mechanism previously described, indicating the reasonability of caging PAM-G matrix in KOH solution for 60 h. Under the condition of 6 M KOH solution for more than 60 h, the skeleton of PAM-G may collapse to hinder the migration of  $\text{K}^+$  and  $\text{OH}^-$  resulting in the capacitance reduction of the supercapacitor.

The kinetics of the gel electrolyte was clarified by the electrochemical impedance measurements. The insert in Fig. 7d shows the EIS model of the assembled quasi-solid supercapacitor. At high frequency, the intercept on the real axis represents the ohmic resistance ( $R_s$ ) and the semicircle corresponds to the charge transfer resistance ( $R_{ct}$ ) at the electrode/electrolyte interface, which is strongly dependent on the abilities of ions transfer and electron conduction [36-37]. At the same time, the straight line displays the diffusive resistance ( $W$ ) when the frequency is low. As can be seen from Fig. 7d, the straight line of the drawing is becoming almost vertical within the extension of 60 h, showing better capacitive behavior of the quasi-solid-state supercapacitor [40]. The charge transfer resistance ( $R_{ct}$ ) of the supercapacitor with PAM-G soaking 60 h is 1.153  $\Omega$ , which is smaller than 7.67, 2.72, 1.28 and 3.89  $\Omega$  of the supercapacitor with PAM-G immersed in the 6 M KOH aqueous solution for 24, 36, 48, and 66 h, respectively. The results demonstrate that  $R_{ct}$  of the quasi-solid-state supercapacitor gradually decreases within the caging time of 60 h and begins to increase when the soaking time exceeds for 60 h, also indicate that the obtained PAM-G electrolyte soaking for 60 h shows the best performances in the field of ions migration.



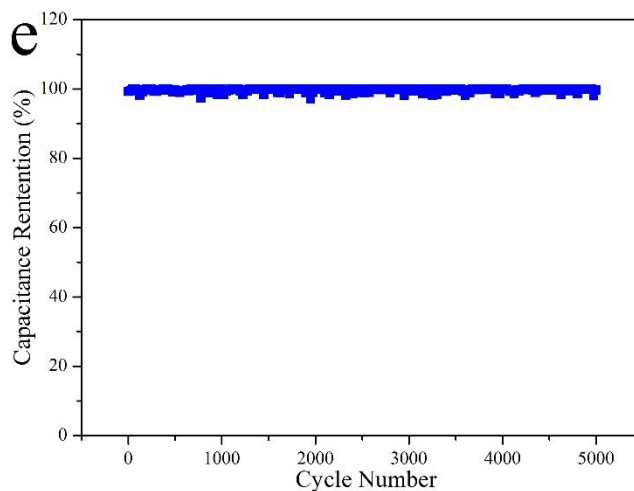


**Figure 8.** (a) CV curves and (b) Galvanostatic charge–discharge profile of the quasi-solid-state supercapacitor, (c) Specific capacitance of the quasi-solid-state supercapacitor at different current densities, (d) Ragone plots of the quasi-solid-state supercapacitor, (e) Cycling stability of the quasi-solid-state supercapacitor at a current density of  $1 \text{ A}\cdot\text{g}^{-1}$ .

The electrochemical performance of the quasi-solid-state supercapacitor which assembled using saturated PAM-G when absorbing KOH aqueous solution for 60 h as electrolyte materials are shown in Fig. 8. Fig. 8a shows the rate-dependent CV curves for the quasi-solid-state supercapacitor over a range of scan rates from 10 to  $150 \text{ mV}\cdot\text{s}^{-1}$ . It can be clearly seen that quasi-rectangular shape can be kept even at high scan rates, proving better stability of the quasi-solid-state supercapacitor. The galvanostatic charge–discharge curves of the quasi-solid-state supercapacitor were also measured at various current densities (Fig. 8b). As can be seen from Fig. 8b, the quasi-solid-state supercapacitor presents a linear galvanostatic charge-discharge curves without obvious ohmic drop at different current densities range from 1 to  $10 \text{ A}\cdot\text{g}^{-1}$ , indicating the quasi-solid-state supercapacitor possess a good capacitive behavior at the different current density. The conclusion that the quasi-solid-state supercapacitor possesses typical electrical double layer capacitor behavior can be obtained through the unique quasi-rectangular of the CV curves and the standard triangle of the galvanostatic charge–discharge curves. As shown in Fig. 8c, the capacitances of the quasi-solid-state supercapacitor gradually decrease with the increase of current density. The gravimetric specific capacitance calculated from the galvanostatic discharge curves is  $196 \text{ F}\cdot\text{g}^{-1}$  at a current density of  $1 \text{ A}\cdot\text{g}^{-1}$ , and maintains  $156 \text{ F}\cdot\text{g}^{-1}$  at  $10 \text{ A}\cdot\text{g}^{-1}$  with a high retention ratio of 80%. To demonstrate the operational characteristics, the energy and power densities in both the electrolytes were calculated according to the following equations [40]:

$$E = \frac{1}{2} C(\Delta V)^2 \quad (4)$$

$$P = \frac{E}{t} \quad (5)$$

Where  $E$  is the average energy density ( $\text{Wh}\cdot\text{kg}^{-1}$ ),  $C$  is the specific capacitance of the symmetric supercapacitor,  $\Delta V$  is the voltage range,  $P$  is the average power density ( $\text{W}\cdot\text{kg}^{-1}$ ) and  $t$  is the discharge time, respectively. As shown in Fig. 8d, a Ragone plot of the quasi-solid-state supercapacitor

displayed maximum power of  $10.06 \text{ kW}\cdot\text{kg}^{-1}$  and energy density of  $28.6 \text{ Wh}\cdot\text{kg}^{-1}$  under the current density of  $10 \text{ A}\cdot\text{g}^{-1}$ . Thus, the optimized PAM-G electrolyte cell performance shows the possibility as safe next generation supercapacitors with a high operating voltage, light weight, and simple design.

Further, the long-term cycling stability is an important performance of supercapacitors [41]. To investigate the cycling stability of the quasi-solid-state supercapacitor, the galvanostatic charge/discharge cycling was studied at a current density of  $1 \text{ A}\cdot\text{g}^{-1}$  in a potential window of 0 to 1 V. As shown in Fig. 8e, the specific capacitance of 5000 cycles only decreases by 2% in comparison with the initial discharge specific capacitance, indicating that the excellent long-term cycling stability of the quasi-solid-state supercapacitor.

**Table 1.** Compared performances of supercapacitor assembled with different gel electrolyte.

Different gel electrolyte	capacitance ( $\text{F}\cdot\text{g}^{-1}$ )	energy density ( $\text{Wh}\cdot\text{kg}^{-1}$ )	capacitance retention
PAM gel electrolyte	196	28.6	98% after 5000 cycles
PMMA based gel electrolyte [42]	178	24.7	85% after 5000 cycles
PVA–LiClO <sub>4</sub> gel electrolyte [43]	112	15	92% after 2500 cycles
PVdF-HFP gel electrolyte [44]	176	26.6	80% after 5000 cycles
IL-b-PE gel electrolyte [45]	150	30	90% after 2000 cycles

The compared performances of the supercapacitors assembled with different gel electrolyte are shown in Table 1. The specific capacitance of the supercapacitor with PAM electrolyte can attain  $196 \text{ F}\cdot\text{g}^{-1}$  which is the highest of the supercapacitors assembled with different gel electrolyte. At the same time, the energy density of supercapacitor with PAM electrolyte can reach  $28.6 \text{ Wh}\cdot\text{kg}^{-1}$  which is much higher than those of supercapacitors assembled with different gel electrolyte [42-45] indicated the possibility of high power charging and discharging. When considered the performance period, the supercapacitor assembled with PAM gel electrolyte can retain the capacitance of 98% after 5000 cycles showing the longest cycle time of all the referenced supercapacitors. In conclusion, the fabricated PAM gel electrolyte has comprehensive application aspect in assembled supercapacitor for the advantages of high capacitance, excellent long-term cycling stability and simple synthesis.

#### 4. CONCLUSION

In summary, a kind of PAM-G electrolyte with high electric conductivity of  $15.06 \text{ mS}\cdot\text{cm}^{-2}$  and three-dimensional structure has been developed by the PAM-G immersed in the 6 M KOH aqueous solution for 60 hours and applied to assemble the quasi-solid-state supercapacitors. As expected, the supercapacitor displays a high specific capacitance ( $C_s$ ) of  $196 \text{ F}\cdot\text{g}^{-1}$  at the charge-discharge current density of  $1 \text{ A}\cdot\text{g}^{-1}$ , high rate capacitance retention ( $156 \text{ F}\cdot\text{g}^{-1}$  remained at  $10 \text{ A}\cdot\text{g}^{-1}$ ), and maximum

power of  $10 \text{ kW}\cdot\text{kg}^{-1}$  along with energy density of  $28.6 \text{ Wh}\cdot\text{kg}^{-1}$  (at  $10 \text{ A}\cdot\text{g}^{-1}$ ). At the same time the quasi-solid-state supercapacitors presents only 2% decrease in capacitance after 5000 cycles under the current density  $1 \text{ A}\cdot\text{g}^{-1}$  showing superior long cycling stability. Meanwhile, the quasi-solid-state supercapacitor can effectively solve the problems of easily leaking, and carrying difficultly, which is often appeared in the supercapacitor with liquid electrolytes. In view of the above advantages, we can foresee the simple assemble process of PAM-G electrolyte can be utilized in wider applications such as flexible or shape memory systems in the future.

#### ACKNOWLEDGEMENTS

The authors acknowledge financial support from National Natural Science Foundation of China (21503202, 61604143, 61774139), Shandong Provincial Natural Science Foundation (ZR2015EM024) and Fundamental Research Funds for the Central Universities (201564002, 201762018).

#### References

1. I. Chung, B. Lee, J. He, R. P. H. Chang, M. G. Kanatzidis, *Nat. Lett.*, 485 (2012) 486.
2. L. Brennan, P. Owende, *Renew. Sust. Energy Rev.*, 14 (2010) 557.
3. X. X. Chen, Q. W. Tang, B. L. He, L. M. Yu, *Energy Conversion*, 126 (2014) 975.
4. X. Wu, P. Liu, L. Ma, Q. Zhou, Y. S. Chen, J. X. Lu, S. Yang, *Sol. Energ Mat. Sol.*, C 152 (2016) 111.
5. F. Pfeffer, J. Eisenlohr, A. Basch, M. Hermle, G. Lee, *Sol. Energ Mat. Sol.*, C 152 (2016) 80.
6. L. Wei, G. Yushin, *Nano Energy*, 4 (2012) 552.
7. Z. Y. Xing, B. Wang, W. Y. Gao, C. Q. Pan, *Nano Energy*, 11 (2015) 600.
8. J. Yan, Q. Wang, T. Wei, Z. G. Fan, *Adv. Energy Mater.*, 4 (2014) 345.
9. J. Zhong, L. Q. Fan, X. Wu, J. H. Wu, G. J. Liu, J. M. Lin, M. L. Huang, Y. L. Wei, *Electrochim. Acta*, 166 (2015) 150.
10. B. Xu, F. Wu, R. Chen, G. P. Cao, S. Chen, Z. Zhou, *Electrochem. Commun.*, 5 (2008) 795.
11. S. Fiorenti, J. Guanetti, Y. Guezennec, S. Onori, *J. Power Source*, 241 (2013) 112.
12. A. Vlad, N. Singh, C. Galande, P. M. Ajayan, *Adv. Energy Mater.*, 5 (2015) 345.
13. A. Gee, F. Robinson, R. Dunn, *Energy Covers. Manage*, 28 (2013) 24.
14. T. Wei, L. J. Zhi, G. Q. Ning, T. Y. Li, F. Wei, *Adv. Funct. Mater.*, 21 (2011) 2366.
15. F. Beguin, V. Presser, A. Balducci, E. Frackowiak, *Adv. Mater.*, 26 (2014) 2219.
16. W. W. Liu, Y. Q. Feng, X. B. Yan, J. T. Chen, Q. J. Xue, *Adv. Funct. Mater.*, 23 (2013) 4111.
17. S. N. Guo, Y. Zhu, Y. Y. Yan, Y. L. Min, J. C. Fan, Q. J. Xu, H. Yun, *J. Power Sources*, 316 (2016) 176.
18. A. Lewandowski, A. Olejniczak, M. Galinski, I. Stepniak, *J. Power Sources*, 195 (2010) 5814.
19. A. Balducci, R. Dugas, P. L. Taberna, P. Simon, D. Plee, M. Mastragostino, S. Passerini, *J. Power Sources*, 165 (2007) 922.
20. Z. Q. Niu, L. Zhang, L. L. Liu, B. Zhu, H. Dong, X. D. Chen, *Adv. Mater.*, 25 (2013) 4035.
21. D. Vonlanthen, P. Lazarev, K. A. See, F. Wudl, A. J. Heeger, *Advanced Materials* 26 (2014) 5095.
22. P. Yang, W. Mai, *Nano Energy*, 8 (2014) 274.
23. Q. Q. Tang, M. M. Chen, G. C. Wang, H. Bao, P. Saha, *J. Power Sources*, 284 (2015) 400.
24. Z. G. Yin, Q. D. Zheng, *Adv. Energy Mater.*, 2 (2012) 179.
25. D. Mecerreyes, *Prog. Polym. Sci.*, 36 (2011) 1629.
26. I. Osada, H. Vries, B. Scrosati, S. Passerini, *Angew. Chem. Int. Ed.*, 55 (2016) 500.
27. X. H. Liu, D. D. Wu, H. L. Wang, Q. Q. Wang, *Adv. Mater.*, 26 (2014) 4370.
28. A. A. Łatoszynska, G. Z. Zukowska, I. A. Rutkowska, *J. Power Sources*, 274 (2015) 1147.

29. C. Z. Meng, C. H. Liu, L. Z. Chen, C. H. Hu, S. S. Fan, *Nano Lett.*, 10 (2010) 4025.
  30. L.Y. Yuan, X. H. Lu, X. Xiao, T. Zhai, J. J. Dai, F. C. Zhang, B. Hu, X. Wang, L. Gong, J. Chen, C. G. Hu, Y. X. Tong, J. Zhou, Z. L. Wang, *ACS Nano*, 6 (2012) 656.
  31. B. G. Choi, J. Hong, W. H. Hong, P. T. Hammond, H. Park, *ACS Nano*, 5 (2011) 7205.
  32. F. H. Meng, Y. Ding, *Adv. Mater.*, 23 (2011) 4098.
  33. A. Lewandowski, M. Zajder, E. Frackowiak, F. Beguin, *Electrochim. Acta*, 46 (2014), 2777.
  34. H. S. Nam, N. L. Wu, K. T. Lee, K. M. Kim, C. G. Yeom, L. R. Hepowit, J. M. Ko, J. D. Kim, *J. Electrochem. Soc.*, 159 (2012) A899.
  35. K. T. Lee, N. L. Wu, *J. Power Sources*, 179 (2008) 430.
  36. Q. W. Tang, J. H. Wu, X. M. Sun, Q. H. Li, J. M. Lin, L. Q. Fan, *Polymer*, 50 (2009) 752.
  37. Q. W. Tang, J. H. Wu, H. Sun, J. M. Lin, S. J. Fan, D. Hu, *Carbohydr. Polym.*, 74 (2008) 215.
  38. N. W. Franson, N. A. Peppas, *J. Appl. Polym. Sci.*, 28 (1983) 1299.
  39. L. F. Chen, X. D. Zhang, H. W. Liang, *ACS Nano*, 6 (2012) 7092.
  40. K. L. Wang, M. Xu, Y. Gu, Z. G. Gu, Q. H. Fan, *J. Power Sources*, 332 (2016) 180.
  41. Y. B. Liu, L. Y. Lin, Y. Y. Huang, C. C. Tu, *J. Power Sources*, 315 (2016) 23.
  42. S. A. Hashmi, A. Kumar, S. K. Tripathi, *Eur. Polym. J.*, 41 (2005) 1373.
  43. N. R. Chodankar, D. P. Dubal, A. C. Lokhande, C. D. Lokhande, *J. Colloid Interf. Sci.*, 460 (2015) 370.
  44. G. P. Pandey, T. Liu, C. Hancock, Y. H. Li, X. S. Sun, J. Li, *J. Power Sources*, 328 (2016) 510.
  45. G. A. Tiruye, D. M. Torrero, J. Palma, M. Anderson, *J. Power Sources*, 326 (2016) 560.
- Rebeca Marcilla

© 2018 The Authors. Published by ESG ([www.electrochemsci.org](http://www.electrochemsci.org)). This article is an open access article distributed under the terms and conditions of the Creative Commons Attribution license (<http://creativecommons.org/licenses/by/4.0/>).